Carbohydrate Polymers 109 (2014) 7–15

Contents lists available at ScienceDirect

Carbohydrate Polymers

journal homepage: www.elsevier.com/locate/carbpol

Electrospun chitosan-based nanocomposite mats reinforced with chitin nanocrystals for wound dressing

Narges Naseri[a], Constance Algan[a], Valencia Jacobs[b], Maya John[b], Kristiina Oksman[a], Aji P. Mathew[a,*]

[a] Division of Materials Science, Department of Engineering Sciences and Mathematics, Luleå University of Technology, 971 87 Luleå, Sweden
[b] CSIR Materials Science and Manufacturing, Fibers and Textiles Competence Area, P.O. Box 1124, Port Elizabeth 6000, South Africa

ARTICLE INFO

Article history:
Received 14 January 2014
Received in revised form 10 March 2014
Accepted 13 March 2014
Available online 26 March 2014

Keywords:
Electrospinning
Chitin nanocrystals
Nanocomposite
Wound dressing
Mechanical properties
Cytocompatibility

ABSTRACT

The aim of this study was to develop electrospun chitosan/polyethylene oxide-based randomly oriented fiber mats reinforced with chitin nanocrystals (ChNC) for wound dressing. Microscopy studies showed porous mats of smooth and beadless fibers with diameters between 223 and 966 nm. The addition of chitin nanocrystals as well as crosslinking had a positive impact on the mechanical properties of the mats, and the crosslinked nanocomposite mats with a tensile strength of 64.9 MPa and modulus of 10.2 GPa were considered the best candidate for wound dressing application. The high surface area of the mats ($35\ m^2\ g^{-1}$) was also considered beneficial for wound healing. The water vapor transmission rate of the prepared mats was between 1290 and 1548 $g\ m^{-2}\ day^{-1}$, and was in the range for injured skin or wounds. The electrospun fiber mats showed compatibility toward adipose derived stem cells, further confirming their potential use as wound dressing materials.

1. Introduction

Dressing materials are used for skin injuries in order to prevent bleeding, keep the wound moist, protect the wound from environmental infections, remove excess exudates and accelerate the healing process. Furthermore, they should be non-toxic and antibacterial because of the direct contact with the wound (Ulubayram, Cakar, Korkusuz, Ertan, & Hasirci, 2001). A porous structure, good barrier properties and oxygen permeability are other desired properties, which need to be taken into account in the manufacturing of dressing materials (Khil, Cha, Kim, Kim, & Bhattarai, 2003).

A large number of biomaterials have been used in wound dressing/healing application (Eich & Stadler, 1999). The use of polymeric nanofibers has attracted considerable interest as an alternative to conventional wound therapy (Turner, 1997) due to high surface area to volume ratio, high porosity, pore size distribution and morphology. These characteristics, which are similar to natural extracellular matrix (ECM), make nanofibers suitable substrates for cell adhesion and proliferation (Li, Laurencin, Caterson, Tuan, & Ko, 2002). Nanofibers prepared from biopolymers activate the fibroblasts that migrate to the dermal layer, which excretes the main constituents of extracellular matrix to heal the injured tissue (Chen, Chang, & Chen, 2008).

One of the methods of producing non-woven nanofiber networks with diameters in the range of several micrometers to tens of nanometers is electrospinning (Herrera, Mathew, Wang, & Oksman, 2011; Jayakumar, Prabaharan, Nair, & Tamura, 2010; Ramakrishna & Fujihara, 2005). The polymer properties, concentration of polymer solution, applied voltage and spinneret diameter can have an impact on, i.e. the morphology and diameter of the produced fibers (Huang, Zhang, Kotaki, & Ramakrishna, 2003; Katti, Robinson, Ko, & Laurencin, 2004). Fibers produced by electrospinning can absorb wound exudates, prevent excessive dehydration and bacterial infection from the wound and facilitate gas permeability; therefore, they have potential for use in wound dressing (Khil et al., 2003; Muzzarelli, 2011).

Different types of chitin- and chitosan-based wound dressing materials are commercially available. Chitin and chitosan in the form of composites, gels, nanofibers, films, non-wovens and scaffolds have been used in order to regenerate wounded tissues (Jayakumar et al., 2011; Muzzarelli et al., 2007; Muzzarelli, 2012) due to their excellent biological and physicochemical properties such as biodegradability, biocompatibility, non-toxicity, antimicrobial and hydrating features. Chen et al. (2008) reported that electrospun chitosan/collagen/PEO nanofibrous membrane

* Corresponding author. Tel.: +46 920 49 3336; fax: +46 920 49 1399.
E-mail address: aji.mathew@ltu.se (A.P. Mathew).

http://dx.doi.org/10.1016/j.carbpol.2014.03.031
0144-8617/

crosslinked by glutaraldehyde vapor is beneficial in wound healing application. They indicated non-cytotoxicity for these nanofibers regarding 3T3 fibroblast growth and in vitro biocompatibility. Since skin is really important in homeostasis and inhibition of microorganisms, chitosan can activate fibroblast proliferation and will aid collagen deposition by releasing N-acetyl-β-D-glucosamine and inducing the high level of hyaluronic acid at the wound location in order to accelerate healing process and scarless wound healing (Jayakumar et al., 2011; Paul & Sharma, 2004).

Nanofibers containing strong antimicrobial agents such as silver nanoparticles (AgNPs) have also been used in wound healing application (Jin, Lee, Jeong, Park, & Youk, 2005). However, the toxicity potential of these nanoparticles in higher concentration has attracted health and ecological concerns (Prabhu & Poulose, 2012). Chitin in the form of highly crystalline nanowhiskers is a bio-based functional additive that has been successfully produced by Marchessault, Morehead, and Walter (1959). It has been used as reinforcement in biopolymers and is a suitable nanoentity for this application (Mathew, Laborie, & Oksman, 2009; Muzzarelli et al., 2007; Paillet & Dufresne, 2001).

The purpose of this study was to develop chitosan-based electrospun mats reinforced with chitin for use in wound dressing application. Spinnability of pure chitosan is challenging due to the polycationic nature and high viscosity of chitosan in solution, and specific intra- and inter-molecular interactions. Indeed, formation of three-dimensional strong hydrogen bonds prevents the free movement of the polymeric chain segments exposed to the electrical field, making the formation of a stable jet problematic (Geng, Kwon, & Jang, 2005; Ohkawa, Cha, Kim, Nishida, & Yamamoto, 2004). In order to overcome this difficulty, synthetic polymers such as polyethylene oxide (PEO) (Duan, Dong, Yuan, & Yao, 2004) and polyvinyl alcohol (PVA) (Zhang et al., 2007) are generally used in the ultrafine fiber production. Zhou et al. (2008) produced carboxyethyl chitosan (CECS)/PVA nanofibers using electrospinning technique. The produced nanofibrous mats showed suitable cell attachment, proliferation and potential for wound dressing application. The current study therefore utilized chitosan/PEO blend as matrix phase and chitin nanocrystals as reinforcing phase. Randomly oriented fiber mats were prepared by electrospinning and the effect of ChNC as reinforcement/functional additive as well as genipin as crosslinking reagent was evaluated. Genipin, a naturally occurring crosslinking reagent obtained from geniposide (extracted from the fruits of Gardenia Jasminoides Ellis), has shown lower cytotoxicity compared to glutaraldehyde in wound dressing materials (Liu, Yao, & Fang, 2008; Sung, Huang, Huang, Tsai, & Chiu, 1998). Mi, Sung, and Shyu (2000) reported that genipin is a promising crosslinking reagent for chitosan, since it can react with the free amino groups even at low concentration. Also, they found that genipin can form intra- and inter-molecular crosslinking networks.

The structural morphology, mechanical properties, thermal stability, water vapor permeability, porosity and cytocompatibility of the electrospun fiber mats were characterized.

2. Experimental

2.1. Materials

Chitosan (Mw = 190,000–310,000 and DD = 75–85%) and polyethylene oxide (Mw ~ 1,000,000 and inhibited with 200–500 ppm BHT) were used as matrix and both polymers were purchased from Sigma–Aldrich GmbH (Germany) in the form of powder.

Crab shell chitin in the form of flakes was purchased from Sigma–Aldrich GmbH (Germany) and was used for isolation of chitin nanocrystals.

Table 1
Compositions of electrospinning solution and spinning parameters.

Sample code	M100	M50ChNC50
Matrix (chitosan/PEO 1:1)	100 wt%	50 wt%
Chitin nanocrystals	–	50 wt%
Acetic acid concentration	50 wt%	50 wt%
Solution concentration	3 wt%	3 wt%
Voltage	25 kV	16 kV
Tip to collector distance	155 mm	130 mm
Flow rate	13 mL/h	10 mL/h

PEO, polyethylene oxide.

Hydrochloric acid with 37% concentration was purchased from Merck KGaA (Germany). Acetic acid 96% for analysis EMSURE® was obtained from Merck KGaA (Germany) and was used as solvent. Genipin and phosphate buffered saline (PBS) were purchased from Sigma–Aldrich GmbH (Germany).

2.2. Methods

2.2.1. Isolation of chitin nanocrystals

Chitin nanocrystals isolated from crab shells using hydrochloric acid hydrolysis were used as reinforcing additive. The procedure for isolation of chitin nanocrystals has been reported by Gopalan Nair and Dufresne (2003). The raw material was boiled and stirred in 5 wt% KOH solution for 6 h in order to remove proteins. The suspension was washed with distilled water and thereafter bleached with chlorite at 80 °C for 6 h. Then, the bleached suspension was washed several times with distilled water followed by bleaching and overnight treatment in 5 wt% KOH, and thereafter concentrated by centrifugation. The purified chitin was hydrolysed using 3 N hydrochloric acid at 80 °C for 90 min under stirring. After the hydrolysis process, the suspension was first centrifuged to remove the excess acid and thereafter the turbid supernatant containing the nanocrystals was collected. The nanocrystal suspension was neutralized by dialysis against deionized water and sonified to individualize the crystals prior to the storage.

2.2.2. Electrospinning of randomly oriented fibrous mats

The electrospinning solutions were composed of chitosan blended with PEO in a 1:1 mass ratio as matrix phase and chitin nanocrystals as reinforcing phase. The final concentration of solutions was 3 wt% and the electrospinning solvent used was 50 wt% aqueous acetic acid. In total, two different materials were produced: (i) unreinforced mats used as control and (ii) chitin-reinforced mats. The material concentrations are shown in Table 1.

The spinning was performed using a Single 150 mm Laboratory Electrospinning Platform (Electrospinz-ES1a), which consisted of a high-voltage supplier, a plastic syringe (10 mL Plastipak Syringe from BD, USA) wherein solution was hosted, linked up to a 200 μL plastic needle (Plastibrand, Germany) by a silicone rubber tube. The solution flow rate was controlled by a syringe pump (Aladdin-1000 from World Precision Instrument, USA) and the capillary was connected to a high-voltage power supply, which was able to produce positive DC voltages up to 30 kV. The electrospinning process was performed at ambient conditions and under the processing parameters shown in Table 1.

2.2.3. Crosslinking of nanocomposite mats

Electrospun mats were crosslinked to enhance the mechanical properties and pH stability. The electrospun mats with and without chitin nanocrystals were treated with a genipin solution to perform crosslinking through the reactive groups. Water-conditioned nanocomposite mats were immersed in a 0.05 mmol/L genipin solution for 16 h at ambient conditions. The mats were rinsed first with distilled water, and then with phosphate buffer saline (PBS)

and finally dried in air at room temperature. The material combinations are shown in Table 1.

2.3. Characterization

2.3.1. Flow birefringence

Flow birefringence was used to study the dispersion of nanocrystals in the electrospinning solutions prior to spinning. The setup consisted of a light source, a magnetic stirrer and two cross-polarized filters. The electrospinning solutions were placed between two cross-polarized filters under stirring and the flow birefringence was captured using a digital camera. The flow birefringence of chitin nanocrystals in water medium was used for comparison of the dispersion.

2.3.2. Viscosity

The shear viscosity of the electrospinning solutions was measured by using a rotating viscometer (Brookfield DV-I Prime) with SC4-21 spindle. The temperature of the solutions was kept at 20 °C by a water jacket and a thermostatically controlled water bath. The measurements were made at multiple spindle rotational speeds in order to determine the rheological behavior of the solutions. Every reading was recorded after 10 spindle rotations to reach equilibrium. For each applied rotational speed, viscosity (cP), shear rate (s^{-1}) and torque (%) values were recorded.

2.3.3. Microscopy

To get an overview of the fiber morphology in order to determine the optimum process parameters, the fibers were collected on glass slides after 1 min electrospinning, and then were observed under a Leica DFC 290 Optical Microscope (OM).

The morphology of as-spun fibers was studied using an Atomic Force Microscope (AFM) Nanoscope V from Veeco, USA, at a resonance frequency of 70 kHz and a spring constant of 1–5 N/m. Electrospun fibers were collected on freshly cleaved mica substrates after 90 s electrospinning. The fiber diameters were determined from the height of fibers.

The structural morphologies of as-spun mats and crosslinked mats were studied with a JEOL JSM-6460LV, USA Scanning Electron Microscope at an acceleration rate of 15 kV. All samples were sputter coated with Au for 50 s at 50 mA to reduce electron charging effects.

2.3.4. Mechanical properties

Mechanical properties of electrospun mats were determined using a Dynamic Mechanical Analyser (DMA) QA 800 from TA Instrument, USA, through uniaxial tensile testing. All samples were tested in tensile mode with a 0.001 N preload at a displacement rate of 100 μm/min at isothermal temperature of 23 °C. Samples were cut in rectangular form and the tested samples were about 30 mm in length, 5 mm in width and 7–20 μm thickness, depending on the composition of electrospun mats. The thicknesses of the fibrous mats were determined using SEM imaging of the cross-section of cryo-fractured films sputter coated with Au. The samples were conditioned in a desiccator with 45% RH for 7 days prior to testing. The results are an average based on at least five measurements for each material.

2.3.5. Thermogravimetric analysis

Thermal stability of fibrous mats was performed using Thermo Gravimetric Analyser (TGA) Q500 from TA Instrument, New Castle, DE, USA. Specimens with weight in the range of 8–10 mg were heated under nitrogen gas in a platinum pan from 30 to 600 °C at a heating rate of 10 °C/min. All samples were dried in the vacuum oven at 50 °C, over night in order to get rid of the moisture.

2.3.6. Water vapor permeability

The moisture permeability of electrospun mats was determined using a Water Vapor Permeability Tester LYSSY L80-4000 from PBI Dansensor, Switzerland, according to the standard ASTM E398-03.

Samples were fixed on self-adhesive test cards and then inserted into the tester. These sample cards were used for measuring water vapor permeability of high permeable materials, since they permit decrease of the surface area of the sample and thus prevent the system from getting saturated. The test cycle was automatically controlled and the system monitored the time taken for the humidity to increase from 9.9 to 10.1%. The resultant value was then converted to $g\,m^{-2}\,day^{-1}$. The test cycle was repeated 3–5 times in the humidity range 9.9–10.1% and the resulting water vapor transmission (WVTR) was reported in $g\,m^{-2}\,day^{-1}$.

2.3.7. Surface area measurement by gas adsorption (BET)

The specific surface areas of the electrospun mats were determined through CO_2 adsorption/desorption isotherms using a Micromeritics ASAP 2020 Surface Area and Porosity Analyzer. The adsorption analysis was performed at 273 K. The specific surface area was calculated using the Brunauer–Emmet–Teller (BET) equation. The samples were degassed at 40 °C for one week prior to the measurement in order to remove adsorbed impurities and moisture.

2.3.8. Cytocompatibility test

In vitro cytocompatibility testing was done in a direct contact test system, where the cells comprising adipose derived (ASCs) stem cells and L929 cell line were seeded through the cell culture dish. The effect of the materials on cell growth and morphology was investigated.

3. Results and discussion

3.1. AFM and flow birefringence

Fig. 1a shows the AFM image of the chitin nanocrystals used for this study. The nanocrystals showed typical rod-shaped morphology with diameters in the range of 10–30 nm, as measured by Nanoscope V software. The lengths were in the range of 400 nm and these results correlate with earlier reports on chitin nanocrystal dimensions found in literature (Gopalan Nair & Dufresne, 2003).

Well-dispersed chitin nanocrystals show flow birefringence in aqueous medium (Fig. 1b). Flow birefringence of chitin nanocrystals in chitosan/PEO solution was observed and compared to flow birefringence of ChNC in water in order to evaluate the dispersion. The flow birefringence pattern of electrospinning solution is visible in Fig. 1c and is not significantly different from the pattern of ChNC in water (Fig. 1b), confirming a well-dispersed system that is stable for electrospinning.

3.2. Viscosity of electrospinning solutions

The rheological properties of the electrospinning solutions were investigated and the results of steady-shear flow are shown in Fig. 2. The shear rate range was slightly different for the two spinning solutions because of the equipment limitation. Accurate measurements were obtained only when the torque reading ranged between 10% and 100%. Out of this range, the spindle rotational speed needed to be reduced or the use of a smaller spindle was required. However, to have comparable results, the same spindle was used for every solution.

It is apparent in Fig. 2 that the viscosity of both electrospinning solutions decreases, while the shear rate increases, suggesting a pseudoplastic non-Newtonian behavior, as it is usually observed for most polymer solutions. The viscosimetric study indicates that

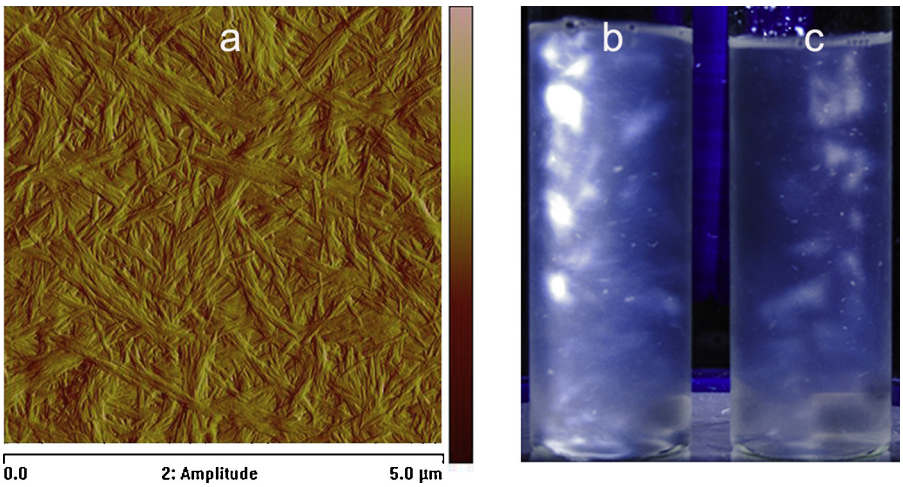

Fig. 1. (a) AFM image of ChNC, (b) flow birefringence of ChNC in deionized water and (c) in diluted electrospinning solution.

the inclusion of chitin nanocrystals within the chitosan/PEO solution significantly decreased the solution viscosity. For instance, at a constant shear rate of 0.465 s^{-1} the viscosity decreased from 21,700 cP to 16,900 cP, i.e. a decrease of 22% after addition of ChNC. This diminution can be explained by the lower concentration of the high-viscosity chitosan content in the solution with chitin nanocrystals (25 wt% of total solute) than in M100 solution (50 wt%) as well as the low viscosity of chitin nanocrystal suspension. The effects of chitin nanocrystals on the chitosan molecular chains are, however, not clear. It was also noticed that as the shear rate increased, the shear-thinning behavior of M50ChNC50 was more pronounced in comparison with M100. The viscosity decreased from 15,033 cP to 8283 cP at shear rate 2.79 s^{-1}, i.e. a reduction of 45%.

3.3. Cytocompatibility of chitin nanocrystals

The short-term cytocompatibility of chitin nanocrystals was studied and the results are shown in Fig. 3. Adipose derived (ASCs) stem cells and L929 cell lines were used for the study, and cell adhesion and growth were tracked for 8 days. Control samples with non-cytotoxic behavior (−K) and samples with cytotoxic behavior (++K) were used for comparison of both types of cells. Chitin nanocrystals isolated from crab shells showed non-toxic impact on adipose derived stem cells and L929 cell line; the cells were growing normally and exhibited normal morphology, as shown in Fig. 3.

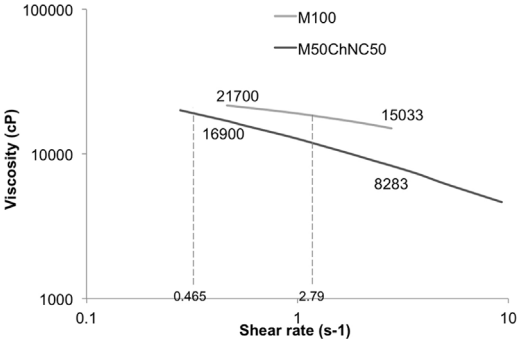

Fig. 2. Viscosity of the electrospinning solutions as a function of shear rate in logarithmic scale.

3.4. Morphology of the nanocomposite fibrous mats

Fig. 4A (a and b) shows electrospun fibers of the reference material (M100) and the composite fibers (M50ChNC50). It can be seen that both fibers have uniform size (diam.) and no beads or other irregularities are visible.

Atomic force microscopy was used to study more detailed structures and sizes of the fibers (Images not shown). The fiber diameters were measured from the height and were in the range of 776–966 nm for the matrix, while in case of chitosan reinforced with chitin nanocrystals the diameters decreased to 223–448 nm. A broad distribution of fiber diameters was noted in both studied materials, probably due to the instability of the whipping jet during the electrospinning process that caused formation of randomly sized fibers. In general, the addition of ChNC shows a trend toward a decrease in fiber diameters, as was also observed in earlier studies (Herrera et al., 2011; Ramakrishna & Fujihara, 2005). This trend may be explained by the decrease in viscosity of the electrospinning solution with the addition of nanoparticles, which encourages stretching of the polymer solution as it travels toward the collector during the electrospinning process, thereby reducing the fiber diameters.

Stable random mats of chitosan/PEO and chitosan/PEO/ChNC were obtained after spinning for about 30 min. Photographs of as-spun mats are presented in Fig. 4B (a and b). Macroscopic defects were visible on the mat made of only matrix (Fig. 4B (a)) due to solvent spraying on the dried deposited fibers. The electrospinning process was quite unstable for M100 mats and uncontrolled whipping of the spinning jet was common during the process. This instability accelerated the travel of the electrospinning solution toward the collecting device, thus preventing complete evaporation of the solvent. Consequently, "wet fibers" and solution droplets spurted onto the collector and destroyed the fibrous structure by re-dissolution of the polymers that constitute the bulk of the freshly dried deposited fibers (i.e. chitosan and PEO).

Electrospinning of M50ChNC50 was more stable and the obtained mat showed homogenous structures (Fig. 4B (b)). The XM100 mat showed large defects (Fig. 4B (c)), whereas crosslinked chitin-reinforced mats showed stable behavior even after crosslinking (Fig. 4B (d)). This indicates that ChNC probably play a role in stabilizing the mats in aqueous medium.

Scanning electron microscopy images of chitosan/PEO fibers and fibers reinforced with chitin nanocrystals are shown in Fig. 5A (a and b), respectively. In both cases a randomly oriented network of electrospun fibers is confirmed. The networks are very loose

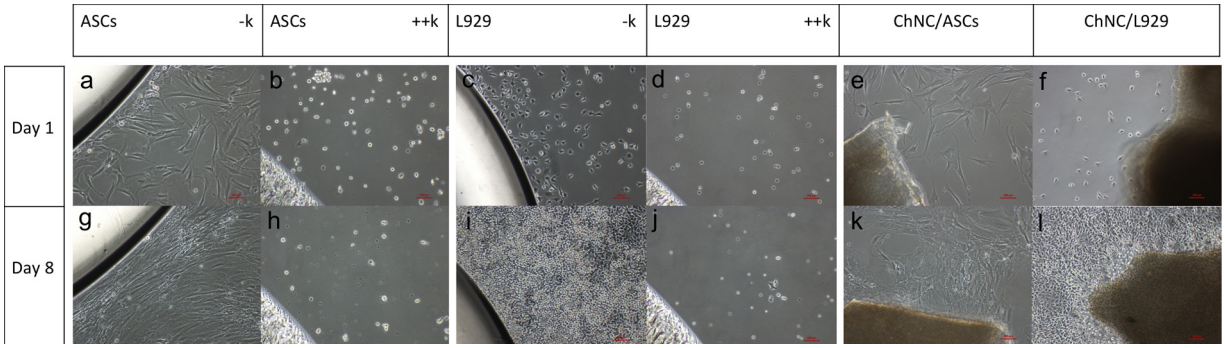

Fig. 3. Cytocompatibility of ChNC toward adipose derived (ASCs) stem cells and L929 cell line. Day 1: (a) non-cytotoxic (−K) control with ASCs, (b) cytotoxic (++K) control with ASCs, (c) non-cytotoxic (−K) control with L929, (d) cytotoxic (++K) control with L929, (e) ChNC with ASCs and (f) ChNC with L929 control with ASCs. Day 8: (g) non-cytotoxic (−K) control with ASCs, (h) cytotoxic (++K) control with ASCs, (i) non-cytotoxic (−K) control with L929, (j) cytotoxic (++K) control with L929, (k) ChNC with ASCs and (l) ChNC with L929 control with ASCs

and have a highly porous structure. No beads were observed for mats containing chitin nanocrystals, supporting the information obtained from OM. It was also possible to see that the nanocomposite fibers with ChNC had lower diameters compared to the matrix fibers, supporting the observation by AFM. Furthermore, both AFM and SEM studies show that chitin-reinforced fibers have surfaces as smooth as fibers made of only the matrix, which indicates a good dispersion of chitin nanocrystals. Fig. 5A (c) shows that crosslinking had a significant impact on the fiber-mat morphology and pore structure. The XM100 mats lost the fiber structure and porosity after crosslinking, probably due to dissolution of PEO in deionized water during crosslinking. The XM50ChNC50 mats (Fig. 5A (d)) were also affected by crosslinking because of the partial dissolution of PEO during crosslinking as well. However, the pore structure was still retained to a large extent in comparison to XM100, possibly due to two reasons: (i) the PEO content is significantly lower (25 wt%) than in the mats without ChNC (50 wt%) and (ii) the presence of 50 wt% of chitin nanocrystals which do not take up water and swell. These differences in the morphology of the mats indicate that chitin nanocrystals provide better moisture stability for the electrospun mats.

Atomic force microscopy was used to observe the as-spun mats and the crosslinked chitin-reinforced mats. XM100 was not studied, as the material lost its fiber structure during crosslinking. Fig. 5B shows the 3D images of the as-spun mats and the crosslinked nanocomposite mat. The images show similar structures as those observed in the SEM study. The as-spun mats showed more rounded fibers and a relatively free porous structure, whereas

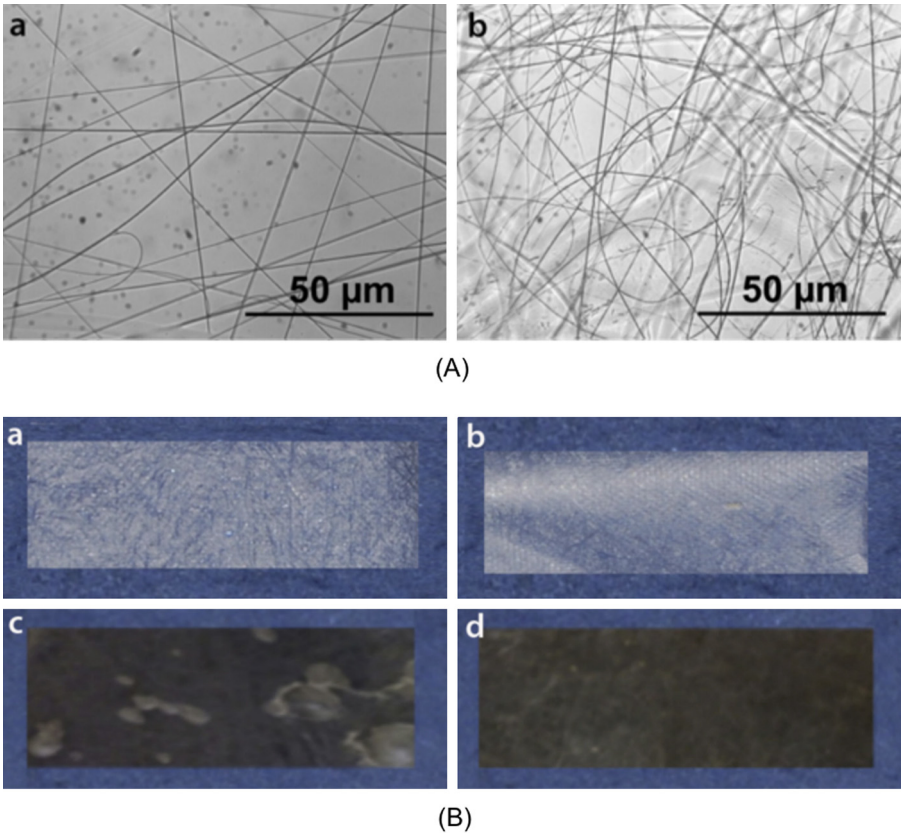

Fig. 4. (A) Optical microscopy images of as-spun fibrous mats: (a) M100 and (b) M50ChNC50. (B) Visual appearance of electrospun mats: (a) M100, (b) M50ChNC50, (c) XM100 and (d) XM50ChNC50

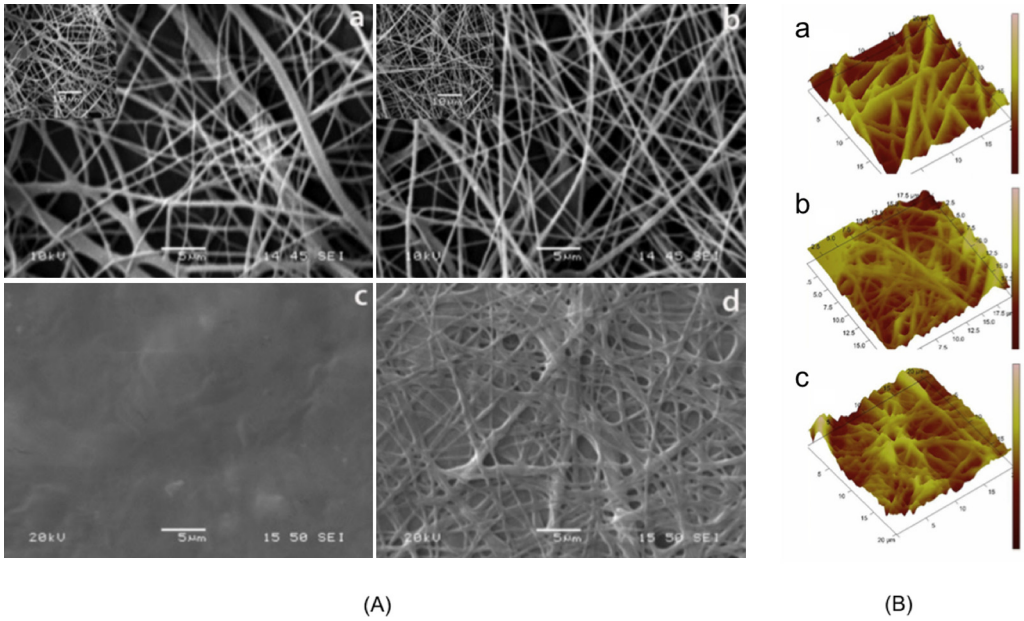

Fig. 5. (A) SEM micrographs showing the surface of randomly oriented fibrous mats: (a) M100, (b) M50ChNC50, (c) XM100 and (d) XM50ChNC50. (B) 3 dimensional AFM images showing the randomly oriented network of (a) M100, (b) M50ChNC50 and (c) XM50ChNC50.

after the crosslinking, the XM50ChNC50 network showed flatter fibers with lower porosity. This shows that the fibrous networks are compacted during crosslinking. This observation was confirmed by the measurement of the mat thickness before and after crosslinking using SEM (images not shown): a decrease of 67% was noticed after crosslinking of as-spun M50ChNC50 mat; however, the fiber structures are retained.

It is important to consider the fact that the current study shows that 50% nanocrystals can be successfully incorporated into chitosan/PEO-based fibers produced by electrospinning. Most of the reported studies on electrospun nanocomposite fibers show lower amounts of nanoparticles in the matrix. Here, the aim was to have a higher amount of chitin nanocrystals, which is expected to provide higher mechanical strength and moisture stability without compromising the non-toxicity and antibacterial properties of chitosan/chitin system.

3.5. Thermal stability

The TGA results of the prepared materials are shown in Fig. 6. Decomposition of chitosan in the nanocomposite mats occurred between 198 and 253 °C, which is in the range of the results reported by Nieto, Peniche-Covas, and Padrón (1991) and Tirkistani (1998). PEO decomposed between 310 and 341 °C, which is also in the range reported by Desai, Kit, Li, and Zivanovic (2008). By comparing the TGA results of pure chitosan and pure PEO reported in the literature (Neto et al., 2005), the presence of both polymers in the blend fibers is confirmed. Thermal analysis of α-chitin nanocrystals, reported by Sriupayo, Supaphol, Blackwell, and Rujiravanit (2005), indicated only one weight loss around 350 °C after the loss of water. In the current study, the initial decrease in weight of about 10% is observed around 100 °C, due to moisture loss for all studied materials, and thereafter the materials showed stable behavior up till 180 °C. This indicates that all the studied mats have the required thermal stability to be used in wound dressing in contact with the body or for steam sterilization (San Juan et al., 2012). It has been observed that inclusion of chitin nanocrystals resulted in a delayed onset temperature of degradation in the case of both uncrosslinked and crosslinked mats. The increased thermal stability in the presence of ChNC may also be related to a well-dispersed nanocomposite material, which benefits from good interaction between chitosan and chitin nanocrystals (Sriupayo et al., 2005). Moreover, for both M100 and M50ChNC50 fibers, crosslinking provided a positive shift for the onset degradation temperature. This indicates the restriction of molecular mobility in the matrix phase in the presence of chitin nanocrystals as well as crosslinking. Furthermore, crosslinking had an impact on the formation of solid phase as char residue, which provides a thermally insulating layer to reduce heat transmission and acts as a diffusion barrier to flammable gases, which explains the high char residue in the crosslinked mats compared to the corresponding uncrosslinked ones (Beyler & Hirschler, 2002).

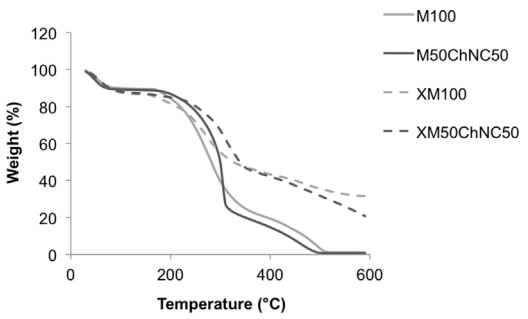

Fig. 6. TGA curves of the fibrous mats.

3.6. Mechanical properties

The tensile properties of the randomly oriented fiber mats were tested and the results are summarized in Fig. 7 and Table 2. Fig. 7

Table 2
Young modulus, Maximum stress and elongation at break of electrospun mats.

Material	Young modulus (GPa)	Tensile strength (MPa)	Max. Strain (%)
M100	0.4 ± 0.1	4.6 ± 0.7	1.3 ± 0.4
M50ChNC50	4.3 ± 0.9	34.9 ± 9.4	0.9 ± 0.2
XM50ChNC50	10.2 ± 2.7	64.9 ± 12.6	0.9 ± 0.1

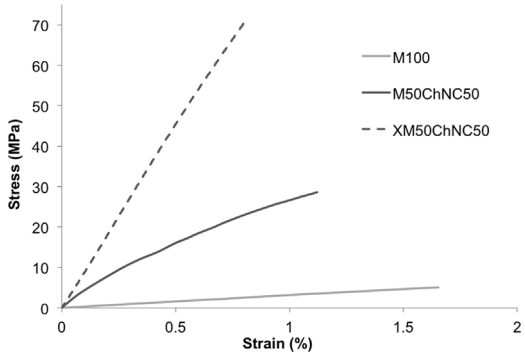

Fig. 7. Stress–strain curves of the electrospun mats.

shows that the ultimate tensile strength and Young's modulus of the mats comprised matrix only were very low and the addition of ChNC in the electrospun fibers increased the Young's modulus and the ultimate tensile strength (Table 2). The tensile strength of the mats increased from 4.6 to 34.9 MPa after inclusion of 50% ChNC, and further increased to 64.9 MPa after crosslinking. The same trend was observed for the Young's modulus, which increased from 0.4 to 4.3 GPa after the addition of ChNC and further increased to 10.2 GPa after crosslinking. However, addition of nanocrystals as well as the crosslinking decreased the strain from 1.3 to 0.9%. The results show that addition of the nanocrystals as well as crosslinking has a positive impact on the mechanical stability of the electrospun mats.

In the current study, the improvement of the mechanical properties is exceptional. The ultimate tensile strength of crosslinked reinforced fibrous mats increases by 1311% and by 2450% for Young's modulus in comparison to as-spun unreinforced mats. The addition of 50 wt% chitin nanocrystals into the electrospun matrix was successful and enhanced the mechanical performance. According to the results reported in Table 2, chitin nanocrystals had considerably greater impact on the mechanical properties compared to crosslinking. The favorable interaction between chitin and chitosan and the possibility to spin the fibers from aqueous medium are also expected to impact the good dispersion of ChNC. Strong interactions between the matrix phase and the nanocrystals through hydrogen bonding might also have led to an improvement

Table 3
Specific surface area and water vapor transmission rates of electrospun mats.

Sample code	BET surface area ($m^2\ g^{-1}$)	WVTR ($g\ m^{-2}\ day^{-1}$)
M100	55	1353
M50ChNC50	59	1290
XM100	36	1548
XM50ChNC50	35	1434

in the structural morphology and mechanical properties (Jacobs et al., 2010). The possibility of crosslinking between matrix and chitin nanocrystals cannot be ruled out. In addition, considerable improvement in mechanical strength and modulus with a decrease in strain at break has been noticed after crosslinking. This is an expected behavior and some earlier reports have shown that crosslinking of a chitosan film using genipin improved the tensile strength but reduced the strain at break considerably (Muzzarelli, 2009). It was also noticed that the mats were flexible despite the decreased strain, probably due to the network structure.

3.7. Functional properties of electrospun mats

Functional characteristics of the prepared mats with respect to the wound dressing were investigated by studying the water vapor permeability, surface area, pore structure and cytocompatibility.

The water vapor transmission rates (WVTR) of different membranes are shown in Table 3. It was observed that all the prepared fibrous mats had a comparable permeability. This was expected, since every mat showed a porous network of entangled electrospun fibers.

An ideal wound dressing must control not only the evaporative water loss from a wound at an optimal rate to avoid excessive dehydration, but also accumulation of wound exudates and, therefore, excess moisture. The water vapor permeation rate for normal skin is 204 $g\ m^{-2}\ day^{-1}$, while WVTR for injured skin can range from 279 to 5138 $g\ m^{-2}\ day^{-1}$, depending on the type of wound (Gu, Wang, Ren, & Zhang, 2009; Mi et al., 2001). The same reports indicate the recommended value of water evaporation for a wound dressing to be around 2500 $g\ m^{-2}\ day^{-1}$. This value is actually the mid-range of moisture loss rates from injured skin and thus is not representative

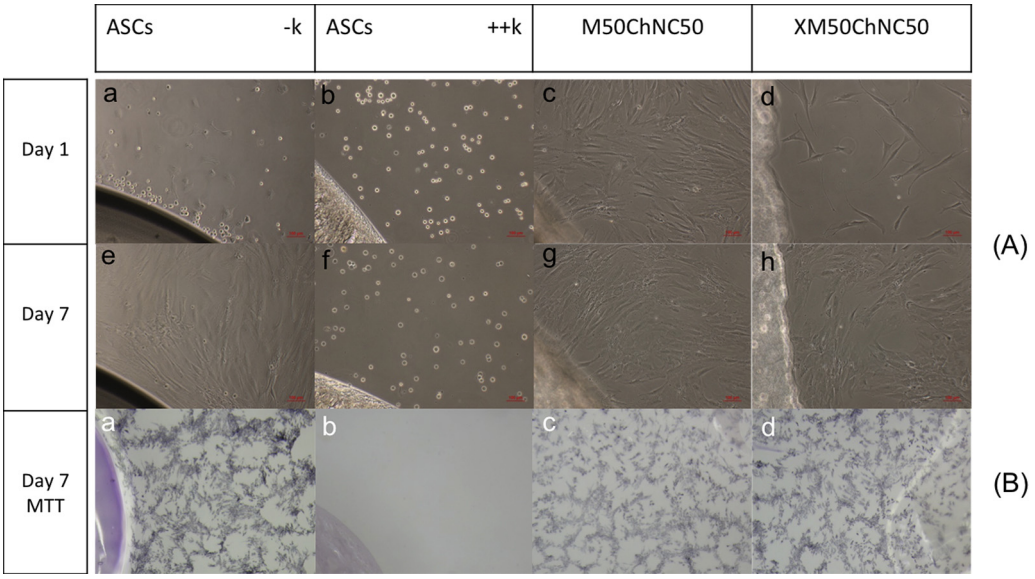

Fig. 8. Cytocompatibility of the mats. (A) Day 1: (a) non-cytotoxic (−K) control, (b) cytotoxic (++K) control, (c) uncrosslinked mats and (d) crosslinked mats with ASCs. Day 7: (e) von-cytotoxic (−K) control, (f) cytotoxic (++K) control, (g) uncrosslinked mats and (h) crosslinked mats with ASCs. (B) MTT stained mats after 7 days: (a) non-cytotoxic (−K) control, (b) cytotoxic (++K) control, (c) uncrosslinked mats and (d) crosslinked mats with ASCs.

of the wound dressing requirements. The WVTR values indicated in Table 3 are lower than this recommended value, but our spun mats are absolutely not limited for wound dressing application. As several types of wound can be found, several types of wound dressing must be used, taking into account the amount of exudates emanating from the wound and the desired moisture content in contact with the wound.

BET surface areas of the electrospun mats are presented in Table 3 and are in the range of 35–59 $m^2 g^{-1}$. The differences in the surface area of as-spun mats are not significant and the same conclusion can be made for the crosslinked mats as well. Therefore, the inclusion of chitin nanocrystals does not have a real impact on the surface area of the fibrous mats. This parameter is mostly affected by the network morphology, as is shown by the decrease in the surface area for both reinforced and unreinforced electrospun mats after crosslinking. From the data collected on the BET surface area of as-spun and crosslinked electrospun fibers, it can be concluded that chemical crosslinking reduces the surface area. This, however, is most likely due to the genipin bonding to the chitosan and thus leading to the compacted fibrous networks with low porosity and lower surface area. The percentage that the BET surface area indicated after crosslinking was a decrease of 34% for chitosan/PEO electrospun fibers and 41% for chitin-reinforced chitosan/PEO fibers. These results correspond with the SEM study, indicating the morphology of spun fibers with loose and porous networks, which decreased after crosslinking. Electrospun fiber membranes with high surface area and microporous structure can stimulate the fibroblast action and proliferation in order to repair injured tissues (Chen et al., 2008). According to Huang et al. (2003), high surface area of 5–100 $m^2 g^{-1}$ is extremely efficient for fluid absorption and dermal delivery. Since the surface area of our materials is in that range, they have potential for cell attachment and proliferation in wound healing.

Cytocompatibility of the mats before and after crosslinking was studied in a direct contact system. The biomaterials with cells were incubated on 37 °C, 5% CO_2 for 7 days with adipose derived (ASCs) stem cells; thereafter, the biomaterials were stained with MTT and investigated for the presence of live cells. According to the cytocompatibility results, which are shown in Fig. 8A and B, non-cytotoxic impact on cell growth and no zone of inhibition were observed compared to the controls. Morphology and cell density of materials are similar to the cells in negative control.

4. Conclusions

Electrospun chitosan-based randomly oriented fibrous mats containing 50 wt% of chitin nanocrystals as reinforcement were successfully prepared and crosslinked using genipin. The results showed that the electrospun porous random mats comprising ChNC were free of any defects because of homogeneous dispersion of ChNC in chitosan matrix, indicating good chemical compatibility between the matrix and the chitin. The addition of chitin nanocrystals improved the moisture stability of the as-spun mats and facilitated water-mediated crosslinking processes. The crosslinked nanocomposite fiber mats with 50 wt% chitin nanocrystals had a high tensile strength of 64.9 MPa and modulus of 10.2 GPa and were at the same time flexible. The mats were also compatible toward adipose derived stem cells after 7 days and can be considered as a potential candidate for wound dressing application.

Acknowledgements

Financial support from VINNOVA under the MNT-ERANET project n-POSSCOG (2011-02071) is acknowledged. The collaboration with CSIR South Africa is supported by the Swedish Research Council (VR) under SIDA project 348-2008-6009 and the National Research Foundation (NRF) under SIDA project UID: 68745. The authors wish to acknowledge Prof. T. Nyokong and Dr. S. Ogunlaja from Rhodes University, South Africa, for the BET studies. Mirjam Fröhlich, EDUCELL and Lenart Girando are acknowledged for cytocompatibility studies.

References

Beyler, C. L., & Hirschler, M. M. (2002). *Thermal decomposition of polymers. SFPE handbook of fire protection engineering* (Vol. 2).
Chen, J. P., Chang, G. Y., & Chen, J. K. (2008). Electrospun collagen/chitosan nanofibrous membrane as wound dressing. *Colloids and Surfaces A: Physicochemical and Engineering Aspects*, *313–314*, 183–188.
Desai, K., Kit, K., Li, J., & Zivanovic, S. (2008). Morphological and surface properties of electrospun chitosan nanofibers. *Biomacromolecules*, *9*, 1000–1006.
Duan, B., Dong, C., Yuan, X., & Yao, K. (2004). Electrospinning of chitosan solutions in acetic acid with poly (ethylene oxide). *Journal of Biomaterials Science, Polymer Edition*, *15*, 797–811.
Eich, D., & Stadler, R. (1999). Differentiated local therapy of chronic wounds with modern wound dressings. *Vasa – Journal of Vascular Diseases*, *28*, 3–9.
Geng, X., Kwon, O. H., & Jang, J. (2005). Electrospinning of chitosan dissolved in concentrated acetic acid solution. *Biomaterials*, *26*, 5427–5432.
Gopalan Nair, K., & Dufresne, A. (2003). Crab shell chitin whisker reinforced natural rubber nanocomposites. 1. Processing and swelling behavior. *Biomacromolecules*, *4*, 657–665.
Gu, S., Wang, Z., Ren, J., & Zhang, C. (2009). Electrospinning of gelatin and gelatin/poly(L-lactide) blend and its characteristics for wound dressing. *Materials Science and Engineering C*, *29*, 1822–1828.
Herrera, N. V., Mathew, A. P., Wang, L. Y., & Oksman, K. (2011). Randomly oriented and aligned cellulose fibres reinforced with cellulose nanowhiskers, prepared by electrospinning. *Plastics, Rubber and Composites*, *40*, 57–64.
Huang, Z. M., Zhang, Y. Z., Kotaki, M., & Ramakrishna, S. (2003). A review on polymer nanofibers by electrospinning and their applications in nanocomposites. *Composites Science and Technology*, *63*, 2223–2253.
Jacobs, V., Anandjiwala, R. D., John, M., Mathew, A. P., & Oksman, K. (2010). Studies on electrospun chitosan based nanofibres reinforced with cellulose and chitin nanowhiskers. In *Anonymous international conference on nanotechnology for the forest products industry 2010* (p. 1378).
Jayakumar, R., Prabaharan, M., Nair, S. V., & Tamura, H. (2010). Novel chitin and chitosan nanofibers in biomedical applications. *Biotechnology Advances*, *28*, 142–150.
Jayakumar, R., Prabaharan, M., Kumar, P. S., Nair, S., Furuike, T., & Tamura, H. (2011). Novel chitin and chitosan materials in wound dressing. *Bio-Medical Engineering*, *13*.
Jin, W., Lee, H. K., Jeong, E. H., Park, W. H., & Youk, J. H. (2005). Preparation of polymer nanofibers containing silver nanoparticles by using poly(N-vinylpyrrolidone). *Macromolecular Rapid Communications*, *26*, 1903–1907.
Katti, D. S., Robinson, K. W., Ko, F. K., & Laurencin, C. T. (2004). Bioresorbable nanofiber-based systems for wound healing and drug delivery: Optimization of fabrication parameters. *Journal of Biomedical Materials Research Part B: Applied Biomaterials*, *70*, 286–296.
Khil, M., Cha, D., Kim, H., Kim, I., & Bhattarai, N. (2003). Electrospun nanofibrous polyurethane membrane as wound dressing. *Journal of Biomedical Materials Research Part B: Applied Biomaterials*, *67*, 675–679.
Li, W. J., Laurencin, C. T., Caterson, E. J., Tuan, R. S., & Ko, F. K. (2002). Electrospun nanofibrous structure: A novel scaffold for tissue engineering. *Journal of Biomedical Materials Research*, *60*, 613–621.
Liu, B. S., Yao, C. H., & Fang, S. S. (2008). Evaluation of a non-woven fabric coated with a chitosan bi-layer composite for wound dressing. *Macromolecular Bioscience*, *8*, 432–440.
Marchessault, R. H., Morehead, F. F., & Walter, N. M. (1959). Liquid crystal systems from fibrillar polysaccharides. *Nature*, *184*, 632–633.
Mathew, A. P., Laborie, M. G., & Oksman, K. (2009). Cross-linked chitosan/chitin crystal nanocomposites with improved permeation selectivity and pH stability. *Biomacromolecules*, *10*, 1627–1632.
Mi, F., Sung, H., & Shyu, S. (2000). Synthesis and characterization of a novel chitosan-based network prepared using naturally occurring crosslinker. *Journal of Polymer Science Part A: Polymer Chemistry*, *38*, 2804–2814.
Mi, F., Shyu, S., Wu, Y., Lee, S., Shyong, J., & Huang, R. (2001). Fabrication and characterization of a sponge-like asymmetric chitosan membrane as a wound dressing. *Biomaterials*, *22*, 165–173.
Muzzarelli, R. A. A. (2009). Genipin-crosslinked chitosan hydrogels as biomedical and pharmaceutical aids. *Carbohydrate Polymers*, *77*, 1–9.
Muzzarelli, R. A. A. (2011). Biomedical exploitation of chitin and chitosan via mechano-chemical disassembly, electrospinning, dissolution in imidazolium ionic liquids, and supercritical drying. *Marine Drugs*, *9*, 1510–1533.
Muzzarelli, R. A. A. (2012). 10.06 – Nanochitins and nanochitosans, paving the way to eco-friendly and energy-saving exploitation of marine resources. In K. Matyjaszewski, & M. Möller (Eds.), *Polymer science: A comprehensive reference* (pp. 153–164). Amsterdam: Elsevier.

Muzzarelli, R. A. A., Morganti, P., Morganti, G., Palombo, P., Palombo, M., Biagini, G., et al. (2007). Chitin nanofibrils/chitosan glycolate composites as wound medicaments. *Carbohydrate Polymers*, *70*, 274–284.

Neto, C. G. T., Giacometti, J. A., Job, A. E., Ferreira, F. C., Fonseca, J. L. C., & Pereira, M. R. (2005). Thermal analysis of chitosan based networks. *Carbohydrate Polymers*, *62*, 97–103.

Nieto, J. M., Peniche-Covas, C., & Padrón, G. (1991). Characterization of chitosan by pyrolysis-mass spectrometry, thermal analysis and differential scanning calorimetry. *Thermochimica Acta*, *176*, 63–68.

Ohkawa, K., Cha, D., Kim, H., Nishida, A., & Yamamoto, H. (2004). Electrospinning of chitosan. *Macromolecular Rapid Communications*, *25*, 1600–1605.

Paillet, M., & Dufresne, A. (2001). Chitin whisker reinforced thermoplastic nanocomposites. *Macromolecules*, *34*, 6527–6530.

Paul, W., & Sharma, C. P. (2004). Chitosan and alginate wound dressings: A short review. *Trends in Biomaterials & Artificial Organs*, *18*, 18–23.

Prabhu, S., & Poulose, E. (2012). Silver nanoparticles: Mechanism of antimicrobial action, synthesis, medical applications, and toxicity effects. *International Nano Letters*, *2*, 1–10.

Ramakrishna, S., & Fujihara, K. (2005). *An Introduction To Electrospinning And Nanofibers*. Singapore: World Scientific Publishing.

San Juan, A., Montembault, A., Gillet, D., Say, J. P., Rouif, S., Bouet, T., et al. (2012). Degradation of chitosan-based materials after different sterilization treatments. In *Anonymous IOP conference series: Materials science and engineering, Vol. 31*.

Sriupayo, J., Supaphol, P., Blackwell, J., & Rujiravanit, R. (2005). Preparation and characterization of a-chitin whisker-reinforced chitosan nanocomposite films with or without heat treatment. *Carbohydrate Polymers*, *62*, 130–136.

Sung, H. W., Huang, R. N., Huang, L. L. H., Tsai, C. C., & Chiu, C. T. (1998). Feasibility study of a natural crosslinking reagent for biological tissue fixation. *Journal of Biomedical Materials Research*, *42*, 560–567.

Tirkistani, F. A. A. (1998). Thermal analysis of some chitosan Schiff bases. *Polymer Degradation and Stability*, *60*, 67–70.

Turner, T. (1997). The development of wound management products. In D. Krasner, & D. Kane (Eds.), *Chronic Wound Care: A Clinical source Book for Healthcare Professionals* (pp. 124–138). Wayne, PA: Health Management.

Ulubayram, K., Cakar, A. N., Korkusuz, P., Ertan, C., & Hasirci, N. (2001). EGF containing gelatin-based wound dressings. *Biomaterials*, *22*, 1345–1356.

Zhang, Y., Huang, X., Duan, B., Wu, L., Li, S., & Yuan, X. (2007). Preparation of electrospun chitosan/poly (vinyl alcohol) membranes. *Colloid and Polymer Science*, *285*, 855–863.

Zhou, Y., Yang, D., Chen, X., Xu, Q., Lu, F., & Nie, J. (2008). Electrospun water-soluble carboxyethyl chitosan/poly(vinyl alcohol) nanofibrous membrane as potential wound dressing for skin regeneration. *Biomacromolecules*, *9*, 349–354.